Pressure Dependence of Magnetic Properties in $La(Fe,Si)_{13}$: Multistimulus Responsiveness of Caloric Effects by Modeling and Experiment

D. Yu. Karpenkov,[1,2,3,*] A. Yu. Karpenkov,[3,4] K. P. Skokov,[1] I. A. Radulov,[1] M. Zheleznyi,[2] T. Faske,[1] and O. Gutfleisch[1]

[1] *Material Science, TU Darmstadt, 64287, Darmstadt, Germany*
[2] *NUST "MISiS", 119049, Moscow, Russia*
[3] *National Research South Ural State University, Chelyabinsk, 454080, Russian Federation*
[4] *Faculty of Physics, Tver State University, 170033, Tver, Russia*

(Received 23 August 2019; revised manuscript received 21 January 2020; accepted 7 February 2020; published 5 March 2020)

For a better understanding of multistimuli-responsive caloric materials with a first-order transition and for optimization of their functional properties, it is necessary to predict the behavior of the material under changes of both magnetic field and pressure. Here, we design and build a special device that can provide a self-consistent set of parameters needed for the comprehensive characterization of multistimuli-responsive functional magnetic materials. Using this scientific instrument, a data set of simultaneously measured magnetization, $M(T)_H$, and volume magnetostriction, $\omega(T)_H$, values are obtained for $LaFe_{11.4}Si_{1.6}$ with a first-order transition. Furthermore, based on simultaneously measured $M(T)$ and $\omega(T)$ dependencies obtained at ambient pressure, we develop an approach that allows the behavior of magnetization under different pressures, $M(T)_P$, to be described analytically. Additional parameters, such as compressibility, $\kappa(T)$; thermal expansion coefficient, $\alpha(T)$; and magnetoelastic interaction or effective magnetovolume coupling constant, C_{MV}, are determined. For verification of our developed model, direct measurements of magnetization under external pressure (up to $P = 1$ GPa) are carried out on the same sample as that used for simultaneous measurement of magnetization and magnetovolume effect. A comparison of simulated $M(T)_P$ dependencies with experimental $M(T)_P$ confirms that our approach provides a more realistic behavior of transition temperature under pressure, $T_C(P)$, than that of the $T_C(P)$ predicted by the Bean-Rodbell model; thus, this approach is more suitable for predicting the behavior of multistimuli-responsive caloric materials with first-order transitions under changes of both magnetic field and pressure.

DOI: 10.1103/PhysRevApplied.13.034014

I. INTRODUCTION

Recent advances in materials science (phase-change magnetic materials [1–5]) and thermal engineering (non-vapor compression cooling technologies [6–8]) help to develop an emerging technology of magnetic refrigeration. However, until now, no commercially competitive magnetic refrigerator has been produced, not even for niche market applications. The overwhelming majority of existing magnetocaloric prototypes use magnetic systems made of permanent magnets (Nd-Fe-B), and, in most cases, such systems provide a magnetic field change, $\Delta\mu_0 H$, of about 0.8–1.2 T [9]. Such magnetic fields lead to a relatively modest cooling power and insufficient thermal operating span, if a magnetocaloric material with a second-order magnetic phase transition (e.g., Gd metal) is used as a solid-state magnetic refrigerant [10–12]. At the same time, if the magnetocaloric material has a first-order magnetostructural transition, a magnetic field change of 1 T can be sufficient for switching the material between paramagnetic-antiferromagnetic and ferromagnetic states, and the discontinuous nature of the first-order transition provides a large isothermal entropy change, ΔS_T, which is typically three to five times higher than that of ΔS_T of the benchmark magnetocaloric material Gd [13].

Severe drawbacks of the first-order transition are, however, inherent thermal and magnetic hystereses, which drastically reduce the cyclic magnetocaloric response [14–17]. Overcoming or circumventing these obstacles will help researchers and engineers to achieve fully reversible adiabatic temperature changes, ΔT_{ad}, and magnetic entropy changes, ΔS_T, closer to the physical limits of the material in low magnetic fields. Recently, it has been shown experimentally [18] that, by applying a uniaxial stress or pressure together with magnetic field, it is possible to actually exploit, rather than avoid, the hysteresis, which, as a consequence, drastically reduces the amount of expensive Nd-Fe-B permanent magnets needed

*karpenkov_d_y@mail.ru

for such a multistimuli magnetic refrigerator. Moreover, the application of external pressure can also reduce the width of the phase transition and cause an enhancement of the magnetocaloric properties [19,20].

For a better understanding of the physics of multistimuli-responsive caloric materials with first-order transitions, and for the optimization of their functional properties, it is necessary to describe analytically and experimentally the magnetoelastic interaction between the magnetic moments and the lattice and to be able to predict the behavior of the material under changes of both magnetic field and pressure [21–23]. Thus, detailed knowledge of additional parameters, such as compressibility, κ; thermal expansion coefficient, α; volume magnetostriction, $\omega(H)_T$; and magnetoelastic interaction or effective magnetovolume coupling constant, C_{MV}, are needed. At the same time, compressibility measurements are often implemented by means of high-pressure x-ray powder diffraction at different temperatures [24,25]. The thermal expansion in a magnetic field, α, and magnetostriction, $\omega(H)_T$, are usually measured on powdered samples by using x-ray or neutron diffraction [26], or on the bulk sample in capacitance or optical dilatometers [27]. The constant of magnetoelastic interaction, C_{MV}, can be calculated by using the Callen-Callen model [28], where spontaneous volume magnetostriction is proportional to the squared magnetization, $\omega(H)_T = \kappa C_{\mathrm{MV}} M^2$ (magnetization M should be obtained by using a magnetometer).

Thus, the precise determination of this set of parameters requires different measurement techniques, and sometimes the sample should be in powdered form; in other cases, it should be in bulk form. Demagnetization factors, temperatures, field sweeping rate, and other experimental conditions can vary from one measurement technique to another, resulting in a not perfectly consistent set of data, especially for samples with very sharp transitions. One of the goals of this work is therefore to design and build a scientific instrument that provides the whole set of parameters needed for the comprehensive characterization of multistimuli-responsive functional magnetic materials.

Here, we select the $LaFe_{11.4}Si_{1.6}$ compound [29,30] to obtain an extensive data set of simultaneously measured magnetization, $M(H)_T$, and volume magnetostriction, $\omega(H)_T$, values. Based on simultaneously measured $M(T)_H$ and $\omega(T)_H$ dependencies obtained at ambient pressure, we develop an approach that allows the behavior of magnetization under different pressures, $M(T)_P$, to be described analytically. This approach consists of five steps. (1) First, by fitting experimental dependencies $M(T)$ and $\omega(T)$ in the framework of mean-field and Bean-Rodbell models, two key parameters of the model, β and η, can be unequivocally identified. (2) Then, using obtained β and η values and $C_P(T)$ experimental data, the temperature dependence of compressibility, $\kappa(T)$, can be determined. (3) In addition, this approach gives us an opportunity to trace temperature dependencies of the magnetovolume coefficient, $\kappa C_{\mathrm{MV}}(T)$. (4) At the next step, combining the spin-fluctuation theory of the itinerant electron metamagnetic (IEM) transition and obtained values of $\kappa C_{\mathrm{MV}}(T)$, the pressure dependence of parameter $\beta(P)$ can be found. (5) Finally, the temperature dependences of magnetization under pressure, $M(T)_P$, can be explicitly calculated and, here, we demonstrate a very good agreement between our analytically obtained and experimentally measured temperature dependencies, $M(T)_P$, for $0 < P < 1.1$ GPa. The procedure flowchart of the proposed approach is presented in Fig. 1.

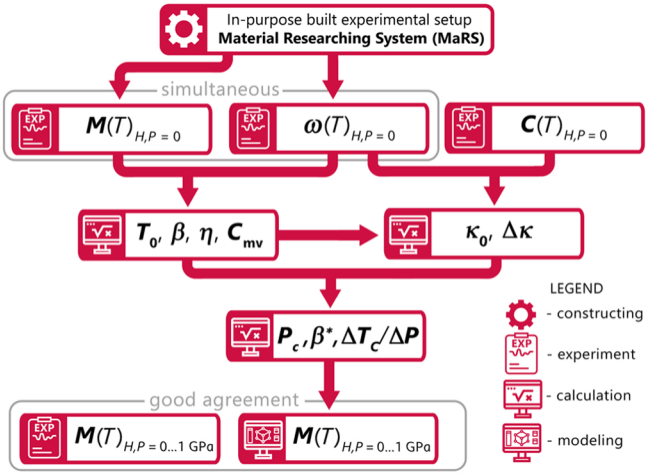

FIG. 1. Procedure flowchart of the proposed approach.

II. EXPERIMENTAL

A. Sample preparation

A $LaFe_{11.4}Si_{1.6}$ ingot of 20 g is produced by induction melting from pure elements. After melting, to ensure homogeneity of the as-cast alloy, the samples are encapsulated in quartz tubes under an Ar atmosphere and then subsequently annealed at 1050°C for 3 h.

The homogenized ingot is then segmented into pieces for subsequent suction casting. Suction casting solves two main problems. The first one is the net shaping of plates of $2 \times 2 \times 1$ mm^3 required for the simultaneous measurement of magnetization and magnetostriction. The second advantage is the reduction of annealing time from one week (typical annealing time for bulk arc-melted or induction-melted samples) down to 12 h for suction-casted plates because of acceleration of the diffusion processes due to a drastic reduction of grain size after quenching. The suction casting of 1 g samples is done by using a rectangular copper mold of $10 \times 4 \times 0.5$ mm^3.

Suction-casted samples consist of predominantly α-Fe and La-rich phases, and therefore, an additional annealing step is required to obtain the magnetocaloric

1:13 phase, which is formed by a peritectic reaction: α-Fe + La-rich $\xrightarrow{1100°C}$ La$(FeSi)_{13}$. So, they are wrapped in Mo foil, sealed in quartz tubes, annealed in a resistance tube furnace at 1100 °C for 12 h, and subsequently quenched in water.

Microstructural characterization and average bulk compositional quantification of the samples are performed using a Philips XL30 FEG scanning electron microscope equipped with an energy-dispersive x-ray system (SEM EDX). The x-ray diffraction (XRD) patterns of the pulverized samples are collected at room temperature using a Stoe Stadi P instrument in transmission mode with a Mo $K\alpha_1$ source radiation ($\lambda = 0.70930$ Å). Rietveld refinement of the XRD patterns is performed using TOPAS Version 6.0 software. Analysis shows that the annealed $LaFe_{11.4}Si_{1.6}$ plates contain 98% of the desired 1:13 phase and approximately 1% of α-Fe and 1% of nonmagnetic $LaFe_{11.4}Si_{1.6}$ phases.

Temperature-dependent XRD experiments are performed in a STOE STADI P diffractometer with Mo $K\alpha_1$ radiation in transmission geometry. For temperature-dependent measurements, an Oxford Cryostream 600 system provides cooling of the $LaFe_{11.4}Si_{1.6}$ sample down to 100 K. The diffraction patterns are analyzed with the FULLPROF suite2 software to extract the lattice parameters and phase fractions. The obtained lattice parameters are used to calculate the unit-cell volume at each temperature.

The heat capacity in magnetic fields of 0, 2, 5, 10, and 14 T from 2 to 350 K is measured using a Quantum Design Physical Properties Measurement System (QD PPMS). Direct measurements of the adiabatic temperature change, ΔT_{ad}, are performed in a home-built experimental setup [17]. The magnetic field is produced by permanent magnets in a Halbach-cylinder configuration. The maximum field in the center of the bore is $\mu_0 H = 1.93$ T. The influence of high pressure on magnetic and magnetocaloric properties of the sample is investigated by using a special high-pressure cell for magnetometry (HMD) for use with a vibrating sample magnetometer (VSM) QD PPMS. The maximum applied pressure is 1.3 GPa.

B. Material researching system (MaRS)

For the simultaneous measurements of magnetization, magnetostriction, and temperature change of $LaFe_{11.4}Si_{1.6}$, a purpose-built experimental setup is designed and built. This scientific instrument greatly enhances the measurement capacity of the commercial VSM option of QD PPMS. Schematics of the device and software interface are shown in Figs. 2 and 3.

The top part of the VSM sample rod is made from a carbon-fiber tube, while a carbon-fiber rod is used for the lower part [Fig. 2(a)]. To avoid signal losses and interference effects, low-temperature low-noise copper twisted wires are used to connect strain gauges and a thermometer

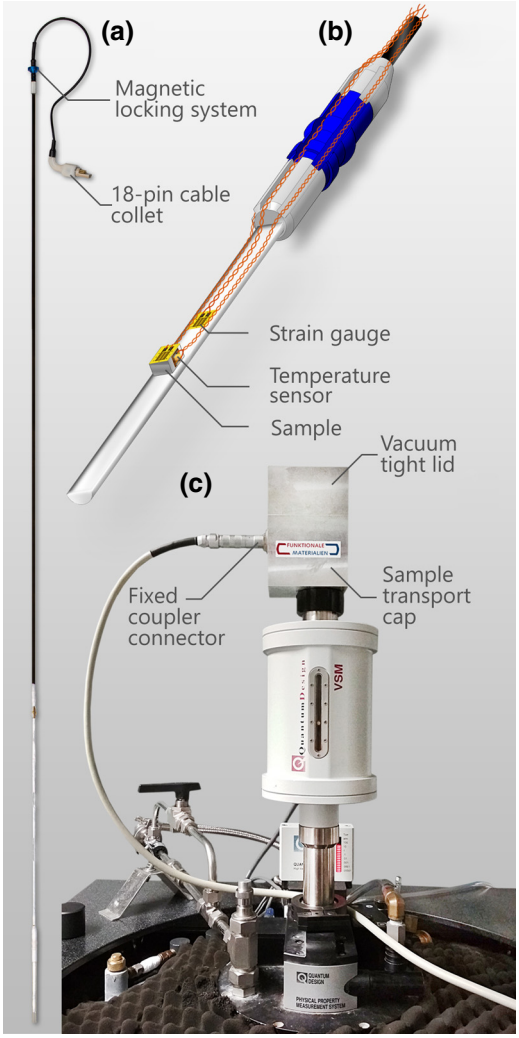

FIG. 2. Experimental setup. (a) Measurement insert and (b) quartz sample paddle with sample and sensors mounted, and (c) transport cap with electrical wiring.

with the data acquisition system. To prevent any damage to the wires by mechanical contact with the VSM guiding system, the wires are placed in a specially designed channel along the sample holder adapter and the carbon-fiber rod. At the top, wires exit the sample rod assembly through a hole in the standard aluminum cap and end with an 18-pin cable collet (Lemo S-connector). The rod is attached to the VSM head through a standard aluminum cap with a magnetic locking system. The homemade sample transport cap [Fig. 3(c)] is similar to the one use with the QD PPMS oven option (P527) and consists of two parts: housing for the fixed coupler Lemo connector and a vacuum tide lid. It has to be mentioned that size of the transport cap is optimized with respect to the number and elasticity of the wires used, because forming the wires in a single-loop spring can significantly increase their life and reduce contact failure due to fatigue caused by vibration.

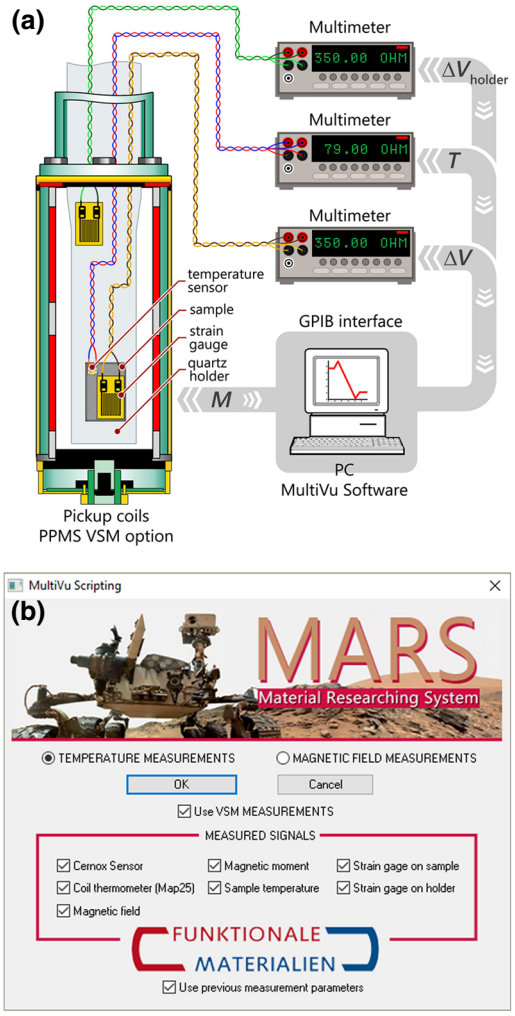

FIG. 3. (a) Schematic of the experimental setup for simultaneous measurements of magnetic moment, magnetovolume change, and temperature change. (b) Screenshot of MaRS software.

The sample holder consists of a quartz half-rod and three-dimensional (3D) printed plastic adapter [Fig. 2(b)]. The Vishay micromeasurement strain gauge (SK-06-031CF-350) is glued to the sample by M-Bond 610 adhesive and the resistive temperature sensors (Cernox CX-1050-BC) are welded to the sample with indium. To compensate for field- and temperature-induced changes in strain-gauge resistivity, an additional reference (SK-06-031CF-350) sensor is attached to the quartz sample holder.

The scheme of the new experimental insert is shown in Fig. 3(a). The VSM pick-up coils, through the bottom "puck" connector of the PPMS, are directly connected to the PPMS control area network (CAN) system. Therefore, the original QD PPMS MultiVu software is used to receive the detected magnetic signal. Three Keithley 2000 multimeters, connected to the MultiVu software through the general purpose interface bus (GPIB), are used to process the signals from two strain gauges and temperature sensors (resistivity four-wire mode). A software module is developed to control the PPMS and communicate with the multimeters [Fig. 3(b)]. The modular design of the PPMS software architecture allows the simultaneous use of the VSM module, together with the multimeter modules, which, in a row, can be adjusted for each specific measurement requirement.

The temperature and field dependencies of magnetization obtained on a bar-shaped sample are identical to those obtained during the simultaneous measurement. The measurement reproducibility and precision is not affected by the additional temperature and stresses introduced by sensors attached to the sample. The results obtained by simultaneous measurements of magnetization and magnetostriction on reference Ni and Terfenol-D ($Tb_{0.3}Dy_{0.7}Fe_2$) samples show that the setup can perform precise measurements in the temperature range 4.2–400 K and magnetic field up to 14 T.

C. Magnetic and magnetocaloric properties of $LaFe_{11.4}Si_{1.6}$

$LaFe_{13-x}Si_x$-type alloys ($1.2 < x < 2.0$) experience a change from first-order to second-order transition types with increasing Si content. The order of the phase transition is changed at $x = 1.6$ [31], and this is the reason why this particular composition is chosen for our experiment: The sample demonstrates all features of magnetic first-order transition: large magnetovolume expansion, ω; remarkable magnetic entropy change, ΔS_T; and a high value of adiabatic temperature change, ΔT_{ad}. At the same time, $LaFe_{11.4}Si_{1.6}$ is very close to the critical point where the first-order transition becomes second order [32]. This allows us to utilize the entropic benefits of the first-order transition without the reduction of the magnetocaloric effect (MCE) due to hysteretic losses. It is also essential that the $LaFe_{11.4}Si_{1.6}$ sample is mechanically stable under thermal and magnetic cycling. This is important for magnetostriction measurements, and good mechanical integrity allows us to avoid the parasitic contribution in the signal during cracking of the sample. For all measurements described here, we use the same $LaFe_{11.4}Si_{1.6}$ sample, which is rectangular shaped ($5 \times 2 \times 0.5$ mm^3) to reduce the impact of the demagnetizing field. In addition, the magnetic field is always applied along the long side of the plate.

The field dependencies of magnetization, $M(H)_T$, measured in our MaRS setup near the first-order transition temperature and in magnetic fields up to 14 T are shown in Fig. 4a. One can see that below 199 K $LaFe_{11.4}Si_{1.6}$ is in a ferromagnetic (FM) state (blue curves) and above this temperature the sample is paramagnetic (PM) in zero field (red curves). A field-induced transition from the PM to FM state is visible with clear first-order features for temperatures of 200, 205, 210, and 220 K; these are characteristic

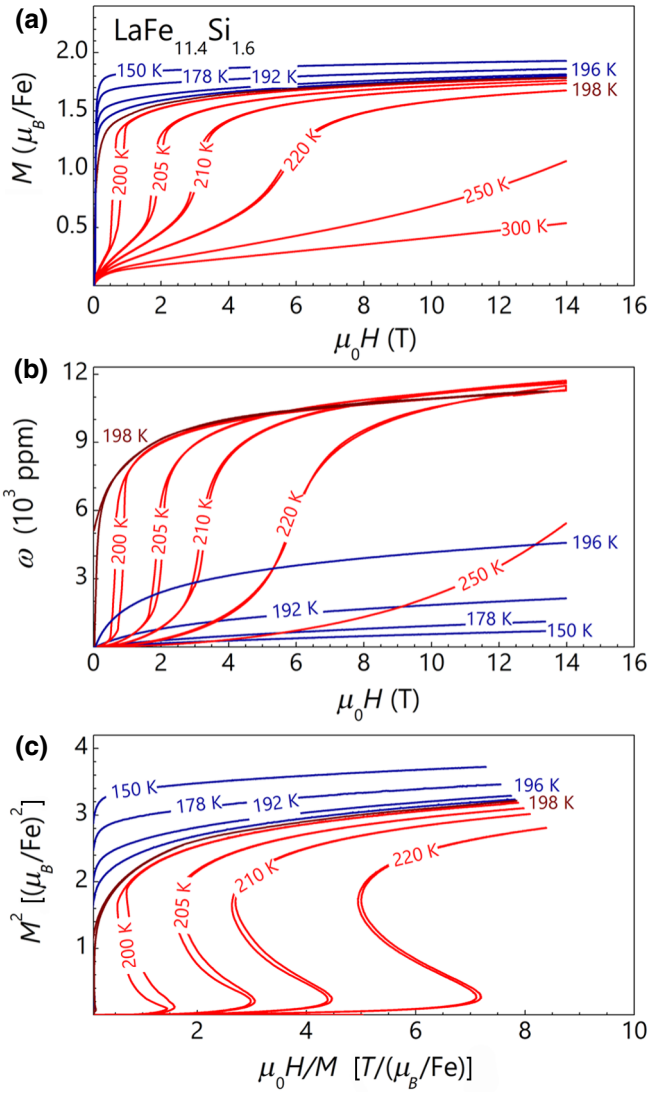

FIG. 4. (a) Field dependences of magnetization, (b) magnetovolume effect, and (c) Belov-Arrott plots of $LaFe_{11.4}Si_{1.6}$ sample.

magnetization curves with a hysteresis between up and down sweeps. The hysteresis width decreases with increasing temperature and the transition is slightly broadened. The critical field of the transition increases with temperature at a rate of 0.25 T/K. The Belov-Arrott plot, in combination with the broadly used Banerjee criterion [33] [Fig. 4(c)], also confirm that our $LaFe_{11.4}Si_{1.6}$ sample is a material with a first-order magnetic phase transition because the $M^2/(\mu_0 H/M)$ curves exhibit negative slopes.

Figure 4b shows the field dependencies of magnetostriction, $\omega(H)_T$, measured simultaneously with magnetization, $M(H)_T$. Field-induced volume expansion in the ferromagnetic region ($T < 196$ K, blue lines) and above the transition ($T > 250$ K, not shown) is rather modest. However, during the transition from ferromagnetic to paramagnetic states, occurring in a temperature range of 199 K $< T <$ 250 K, in a magnetic field of up to 14 T, one can see that it is accompanied by a large volume expansion, $\Delta V/V$, of 1.1% [Fig. 4(b), red curves].

Figures 5(a) and 5(b) depict the temperature dependencies of magnetization, $M(T)_H$, and relative volume change, $\omega(T)_H = [V(T) - V(300\ \text{K})]/V(300\ \text{K})$, simultaneously measured in five selected magnetic fields by using the MaRS setup. Similar to the field dependencies shown in Fig. 4, $M(T)_H$ and $\omega(T)_H$ clearly show that the transition to the ferromagnetic state is accompanied by a lattice expansion typical for materials with an itinerant electron metamagnetic phase transition. The red circles in Fig. 5(b) correspond to the relative changes of the lattice parameter a, as measured by x-ray diffractometry.

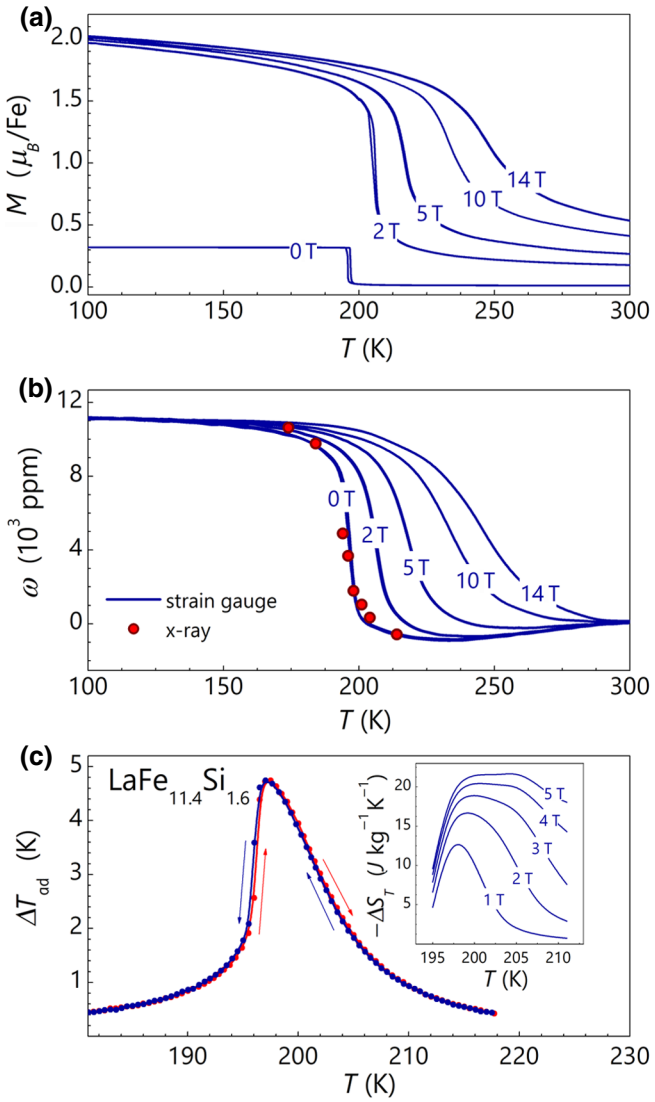

FIG. 5. (a) Temperature dependences of magnetization, (b) temperature dependences of relative volume change of $LaFe_{11.4}Si_{1.6}$ sample at different fields (red circles show the XRD data). (c) Temperature dependences of ΔT_{ad} ($\mu_0 H$=1.9 T) and ΔS_M (inset) of $LaFe_{11.4}Si_{1.6}$ sample.

One observes good agreement between both experimental techniques. The simultaneously obtained $\omega(H)_T$, $M(H)_T$, $M(T)_H$, and $\omega(T)_H$ dependencies shown in Figs. 4(a), 4(c), 5(a) and 5(b) are necessary for further simulation of the temperature dependences of magnetization under pressure, $M(T)_P$.

To directly evaluate the MCE properties of our $LaFe_{11.4}Si_{1.6}$ sample, ΔT_{ad} versus temperature curves are obtained under magnetic field change $\Delta\mu_0 H = 1.9$ T for both heating and cooling protocols, as shown in Fig. 5(c). The maximum value of adiabatic temperature change is determined to be 5 K. The isotheral entropy change, ΔS_T, is calculated from $M(T)_H$ dependencies using the Maxwell relation [see inset in Fig. 5(c)]. The ΔS_T in a magnetic field of 2 T is evaluated to be 16.5 $J\,kg^{-1}\,K^{-1}$. Both ΔS_T and ΔT_{ad} values obtained on our $LaFe_{11.4}Si_{1.6}$ suction-casted plate are typical for samples with first-order transitions near the critical point [2].

III. RESULTS AND DISCUSSIONS

A. Model of pressure impact on magnetic properties

To describe the relationship between applied pressure and variation in magnetic properties, the Bean–Rodbell model can be used as a basic starting point [34–36]. Here, the dependence of the exchange interaction on the interatomic distance is phenomenologically described via the dependence of the critical temperature on the volume change. Bean and Rodbell have suggested that the volume dependence of the Curie temperature can be estimated as

$$T_C = T_0[1 + \beta\omega], \tag{1}$$

where T_C and T_0 are the Curie temperatures of the low-temperature and high-temperature phases, respectively; $\omega = (V - V_0)/V_0$ is the relative volume change, where V_0 is the volume of the high-temperature phase without exchange interactions. β is a dimensionless parameter, characterizing the sensitivity of the exchange interaction on the sample volume.

The Bean–Rodbell model is developed based on the assumption that the ferromagnetic interaction between magnetic moments is localized on each atom site, and the magnetization is described by the Brillouin function for the localized effective magnetic moment, J. At the same time, as investigated in our work, $LaFe_{11.4}Si_{1.6}$ is an itinerant magnet and the magnetically active (unpaired) $3d$ electrons must be considered as delocalized or itinerant electrons. In this case, the spontaneous magnetization is the result of spontaneous spin splitting of the $3d$-$4s$ hybridized electron bands. Assuming that each electron has a spin-only magnetic moment, μ_B, the net magnetization of the metal can be expressed as a difference in the population of the spin-up and spin-down bands. Eventually, for the itinerant magnet, we should use the number of uncompensated for electrons, $N^* = n^+ - n^-$, and spin, $S = ½$ ($\mu_{eff} = \mu_B$), instead of the number of atoms, N, and effective magnetic moment, J, per atom, as suggested in the Bean-Rodbell model.

Taking this assumption within the molecular-field approximation, the Gibbs energy, G, per gram of magnetic material can be written as [35]

$$G = -\frac{1}{2}Nk_BT_C\sigma^2 + \frac{\omega^2}{2\kappa} - TS_{lattice} - TNk_B \times\left[\ln 2 - \frac{1}{2}\ln(1-\sigma^2) - \sigma\tanh^{-1}\sigma\right] - HM_{sat}\sigma + P\omega, \tag{2}$$

where κ is compressibility, N is the number of uncompensated for electrons per unit volume, k_B is the Boltzmann constant, $\sigma = M_s(T)/M_s(0)$ is a reduced spontaneous magnetization, α is a thermal expansion coefficient, $S_{lattice}$ is the entropy of the crystal lattice, and M_{sat} is the saturation magnetization.

One can see that G is a function of two variables, σ and ω, and to find the equation of state of the system with magnetovolume interactions, we should minimize the Gibbs free energy with respect to both variables. First, minimizing the Gibbs free energy by volume, we obtain the expression for the relative volume change:

$$\omega = \frac{1}{2}Nk_B\kappa T_0\beta\sigma^2 + \int \alpha dT - \int \kappa dP, \tag{3}$$

Since compressibility and the thermal expansion coefficient are constant, the last two integrals in Eq. (3) can be replaced by αT and κP terms. It can be seen that, in the framework of the Bean-Rodbell model, the change in volume can be ascribed to changes in t magnetization, crystal lattice, and external pressure. In the zeroth magnetic field ($\sigma = 0$), the shift of the phase transition can be found from

$$T_C = T_0[1 - \beta\kappa P]. \tag{4}$$

We can now replace ω in Eq. (2) by using Eq. (3) and then we can minimize the Gibbs free energy with respect to σ. The result can be conveniently expressed as

$$\frac{T}{T_0} = \frac{\sigma\left(1 + \eta\frac{\sigma^2}{3} - \kappa P\beta\right) + \frac{M_{sat}H}{Nk_BT_0}}{\tanh^{-1}\sigma}, \tag{5}$$

where

$$\eta \equiv \frac{3}{2}Nk_B\kappa T_0\beta^2. \tag{6}$$

Equation (5), obtained by Bean and Rodbell, will be used in the following for the determination of the temperature dependence of σ as a function of temperature, T; external field, H; and pressure, P.

The main problem with straightforwardly using Eq. (5) consists of a rather broad set of additional parameters, such as T_0, compressibility κ, and dimensionless parameters η and β. Moreover, some of these parameters are not constants, but temperature-dependent and field-dependent variables. All of these parameters should be unequivocally and consistently determined before we can use Eq. (5) for the calculation of temperature dependences of magnetization under pressure, $M(T)_P$. Thus, the value of the T_0 parameter in Eq. (5) can be extracted from the experimental $M(T)_H$ dependencies obtained at ambient pressure. In addition, in the framework of molecular-field theory, parameter β (see Sec. III B) can be found. Using this parameter β, parameter η can be calculated using Eq. (5) (see Sec. III C).

The experimental evaluation of the compressibility κ is rather complicated, because compressibility measurements are often implemented by means of high-pressure x-ray powder diffraction at different temperatures, which are often inaccessible and give rather scattered results. The compressibility can be calculated by using the sound velocity value, but ultrasonic detection of the elastic moduli in the La(Fe, Si)13 system with the first-order phase transition are almost impossible due to scattering of sound waves on defects (cracks) caused by giant spontaneous magnetostriction. Despite all this, to understand the dependence of magnetic properties on pressure in the vicinity of the phase transition, an accurate evaluation of $\kappa(T)$ is a crucial task, because it is not a constant, but it should possess a sharp peak at the transition [37]. Therefore, in Sec. III D, we describe our alternative approach for exploration of the temperature dependence of the compressibility $\kappa(T)$.

The β parameter in the Bean-Rodbell model is introduced as a constant [35]:

$$\beta = -\frac{1}{\kappa T_0}\left(\frac{dT_C}{dp}\right). \tag{7}$$

It is shown [38–40] that in La(FeSi)13 alloys the transition temperature is depressed significantly with pressure, however, the ratio dT_C/dp is not a constant and increases with pressure. Hence, the parameter β in Eq. (7) has to be dependent on pressure. Although the Bean–Rodbell model predicts the enhancement of the first-order phase transition under pressure, it cannot describe the nonlinear pressure dependence of transition temperature by taking β as a constant. Thus, to predict the magnetic behavior of the material under pressure, $M(T)_P$, we should determine the pressure dependence of parameter β (see Sec. III F). As an intermediate step (Sec. III E), the temperature dependence of the magnetovolume coefficient, C_{MV}, versus T can be also evaluated. Finally (Sec. III G), Eq. (5), with such determined T_0, $\beta(P)$, η, $\kappa(T)$, and $C_{\mathrm{MV}}(T)$ parameters, can be applied for the simulation of $M(T)_P$.

B. Molecular-field approach and parameter β

To unambiguously define parameter β, which is needed for further simulations, we combine molecular-field theory (MFT) with the Bean-Rodbell model. Since, in our particular case, the La(Fe, Si)13 compound can be considered as an itinerant magnet because of zero magnetization of the rare-earth-element sublattice, we should use spin $S = ½$ instead of an effective magnetic moment, J, per atom. In turn, MFT should be adapted to avoid inconsistencies in the developed approach; hence, the Brillouin function can be simplified to the form of a hyperbolic tangent.

Thus, based on molecular-field theory, we can calculate the temperature dependence of magnetization as follows:

$$\sigma = \tanh[(H_{\mathrm{eff}} + H)\mu_B/k_BT], \tag{8}$$

where $H_{\mathrm{eff}} = \lambda N \mu_B \sigma$ is the molecular field, the parameter of molecular field λ can be written as $\lambda = k_B T_C/(N\mu_B^2)$; $N = 1.6 \times 10^{22}$ is the number of uncompensated for electrons per unit volume. The advantage of this approach is that it consists of very few parameters necessary for the calculation of $\sigma(T)$ dependencies. For these purposes, from an experiment, we should know only the Curie temperature, T_C, which determines parameter λ.

According to Bean and Rodbell, T_C can be written as Eq. (1) and the λ can be written as

$$\lambda = \frac{k_B T_0(1 + \beta\omega)}{N\mu_B^2}. \tag{9}$$

The transition temperature T_0 of a high-temperature phase with an undisturbed volume V_0 can be determined by using the Curie–Weiss law and the temperature dependence of inverse susceptibility, $1/\chi(T)$. From a linear approximation [red solid line in Fig. 6(a)], we find that $T_0 = 196$ K.

Figure 6(b) shows the experimental data of the temperature dependences of the relative volume change, $\omega(T)_{H=0}$, in the zeroth field (solid blue line), whereas the normalized spontaneous magnetization, $\sigma(T)_{H=0}$, obtained from the field dependences of magnetization by using an Arrott plot is shown in Fig. 6(c) as black circles. Using experimental values of $\omega(T)_{H=0}$, $T_0 = 196$ K, and $N = 1.6 \times 10^{22}$, a fitting of experimental $\sigma(T)_{H=0}$ is done by using Eq. (8) with β as a fitting parameter. The calculated $\sigma(T)$ curve with $\beta = 15$ is shown in Fig. 6(c) as a solid blue line. One can see good agreement between experimental and simulated data; hence, the received value of $\beta = 15$ is used for further calculations at ambient pressure.

To illustrate, in detail, how the molecular-field approach works, the results of additional simulations for two nondeformable systems with two different constant volumes, V_0 ($\omega = 0$, $\beta = 15$) and V_1 ($\omega = 0.011$, $\beta = 15$), are shown in Fig. 6(c) as orange (V_0) and red (V_1) dashed lines. These two volumes are taken from experimental $\omega(T)$ data: V_0 corresponds to the lattice in an undisturbed paramagnetic

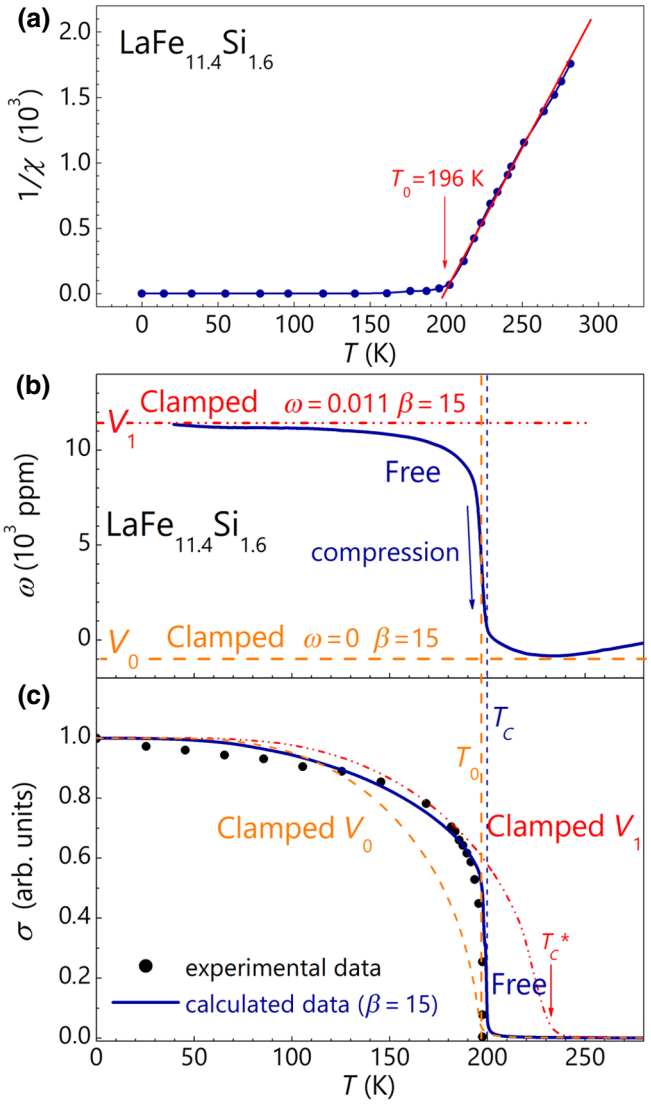

FIG. 6. (a) Temperature dependence of inverse magnetic susceptibility. (b) Temperature dependence of relative volume change of $LaFe_{11.4}Si_{1.6}$ sample at zero field. (c) Reduced spontaneous magnetization versus temperature. Solid blue, dashed orange, and red lines are modeling curves for the parameters $\beta = 15$; black circles are experimental data.

state, whereas V_1 describes the system in a ferromagnetic state with larger volume due to magnetovolume interactions. If we use Eq. (8), keeping volume V_0 fixed at all temperatures, then upon heating from low temperatures we can observe a smooth decrease of the magnetization to zero at a temperature of $T_0 = 196$ K ($T_C = T_0$). For the same system with increased constant volume V_1 ($\omega = 0.011$), the decrease in magnetization will be slower, since its Curie temperature, $T_C = T_0(1 + \beta\omega)$, will be higher, and for $\beta = 15$ the value is $T_C{}^* = 228$ K. In the case of a freely deformable system, the temperature behavior of magnetization will be more complex, since the spontaneous volume magnetostriction, $\omega(T)_{H=0}$, is not constant over the entire temperature range. In such a way, we can conclude that parameter β obtained in framework of the molecular-field approach is very relevant for the simulation of $\sigma(T)$ dependencies of materials with a large magnetovolume effect.

C. Parameter η

Parameter β, as determined in Sec. III B, allows us to find parameter η in framework of the Bean-Rodbell model. Indeed, if magnetic field and pressure are zeroth order, spontaneous magnetization in Eq. (5) depends only on T_0, β, and η. T_0 and β arere found in Sec. III B.

The graphical solutions of Eq. (5) for various values of parameter η ($P = 0$, $H = 0$) are plotted in Fig. 7(a) as red lines. The best fit of the experimental curve, shown with blue circles, corresponds to the parameter $\eta = 1.25$. In general, the η parameter defines the order of the phase transition: if $\eta \leq 1$, the transition is second order and, if $\eta > 1$, the transition is first order. The obtained value of η parameter, $\eta > 1$, indicates the first-order phase transition in the $LaFe_{11.4}Si_{1.6}$ compound.

D. Temperature dependence of compressibility

Since in a framework of the Bean–Rodbell model the compressibility is assumed to be constant, the determined

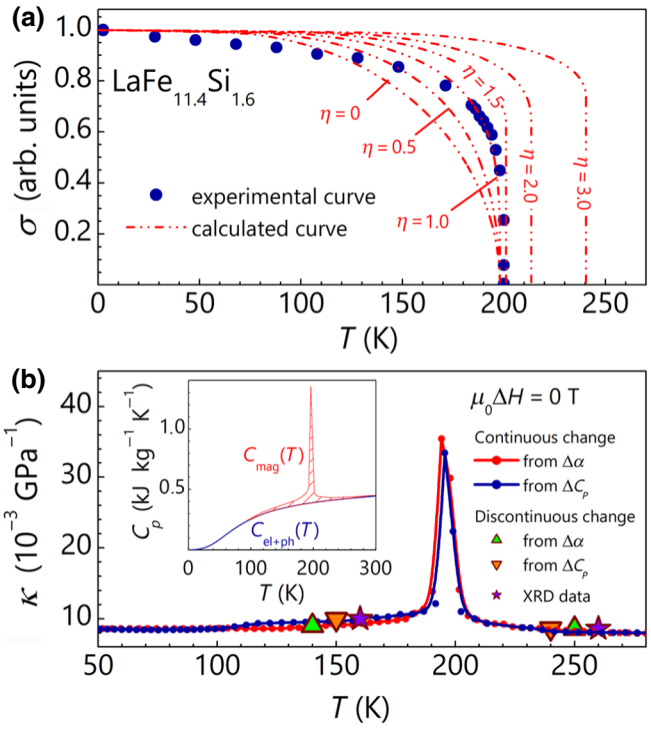

FIG. 7. (a) Reduced spontaneous magnetization versus temperature for different values of parameter η. (b) Temperature dependence of the compressibility for $LaFe_{11.6}Si_{1.4}$. Inset: temperature dependence of specific heat for $LaFe_{11.6}Si_{1.4}$.

value, $\eta = 1.25$, allows us to find such compressibility in the ferromagnetic state as $\kappa_0 = 8.6 \times 10^{-3}$ GPa^{-1} by using Eq. (6). However, in reality, the compressibility drastically changes with temperature near the first-order magnetostructural transition [16]. To calculate $\kappa_0 + \Delta\kappa(T)$, we use two thermodynamic relations: first, between κ and thermal expansion coefficient α [Eq. (14)], and, second, between κ and specific heat, C_P [Eq. (15)]. Below, we show how these Eqs. (14) and (15) can be derived.

According to the Ehrenfest classification, first-order phase transitions have discontinuities in the first derivatives of Gibbs free energy, G, $(\partial G/\partial T)_P = -S$ and $(\partial G/\partial P)_T = V$. Moreover, in theory, being second derivatives of Gibbs energy, heat capacity, C_P, and compressibility, κ, are not defined at the transition temperature. However, this discontinuity is the case only for an ideal first-order phase transition occurring infinitely fast at constant T, P, and H. Actually, all available experimental data (e.g., Fig. 5) show smooth curves of volume and entropy changes of the entire sample. This observable continuity at the transition happens partially due to phase coexistence during the transition and partially owing to slight inhomogeneity of the material. Such smoothness of the experimentally obtained thermodynamic variables measured at the first-order transition allow us to use, for example, the thermodynamic Maxwell relations based on the first derivatives of free energy, instead of using the Clausius-Clapeyron equation, where the discontinuous steplike changes of ΔM, ΔV, ΔS, etc. must be taken into account. Such practice is commonly used, for instance, for evaluation of magnetic entropy changes occurring at the field-induced first-order transition (see, e.g., [41–43]).

Thus, to obtain a reasonable shape of compressibility maxima near the first-order transition, $\kappa_0 + \Delta\kappa(T)$, we can use an approach based on continuous changes of all thermodynamic variables. Let us denote, by the letters A and B, two neighboring states during the smooth first-order transition with temperatures T_A and T_B and pressures P_A and P_B. Since the entropy and volume macroscopically change continuously, we can write

$$dS_A(P_A, T_A) = dS_B(P_B, T_B), \tag{10a}$$

$$dV_A(P_A, T_A) = dV_B(P_B, T_B). \tag{10b}$$

Taking a total differential and by multiplying both parts of Eq. (10a) by T and Eq. (10b) by $1/V$, we get

$$\left[T\left(\frac{\partial S_A}{\partial T}\right)_P - T\left(\frac{\partial S_B}{\partial T}\right)_P\right] dT + T\left[\left(\frac{\partial S_A}{\partial P}\right)_T - \left(\frac{\partial S_B}{\partial P}\right)_T\right] dP = 0, \tag{11a}$$

$$\frac{1}{V}\left[\left(\frac{\partial V_A}{\partial T}\right)_P - \left(\frac{\partial V_B}{\partial T}\right)_P\right] dT + \left[\frac{1}{V}\left(\frac{\partial V_A}{\partial P}\right)_T - \frac{1}{V}\left(\frac{\partial V_B}{\partial P}\right)_T\right] dP = 0, \tag{11b}$$

where dT can be treated as $\Delta T = T_B - T_A$ and dP is $\Delta P = P_B - P_A$. Using Eqs. (11a) and (11b) and thermodynamic relations

$$T\left(\frac{\partial S}{\partial T}\right)_P = C_P, \tag{12a}$$

$$\left(\frac{\partial S}{\partial P}\right)_T = -\left(\frac{\partial V}{\partial T}\right)_P = -V\alpha, \tag{12b}$$

$$\kappa = -\frac{1}{V}\left(\frac{\partial V}{\partial P}\right)_T, \tag{12c}$$

one can obtain

$$\Delta C_P \Delta T = TV\Delta\alpha\Delta P, \tag{13a}$$

$$\Delta\kappa\Delta P = \Delta\alpha\Delta T. \tag{13b}$$

It must be noted that $\Delta C_P = C_{P,T_B} - C_{P,T_A}$, $\Delta\alpha = \alpha_{T_B} - \alpha_{T_A}$, and $\Delta\kappa = \kappa_{P_B} - \kappa_{P_A}$.

Since in the vicinity of the transition, $\Delta P/\Delta T$ is only dP/dT_C, and it follows that

$$\Delta C_P = T_C V\Delta\alpha\left(\frac{dP}{dTc}\right), \tag{14}$$

$$\Delta\kappa = \Delta\alpha\left(\frac{dT_C}{dP}\right), \tag{15}$$

from Eqs. (14) and (15), we find that

$$\Delta\kappa = \frac{\Delta C_P}{T_C V}\left(\frac{dT_C}{dP}\right)^2. \tag{16}$$

Thus, to obtain $\Delta\kappa(T) = \kappa(T_B) - \kappa(T_A)$, we can use either experimental dependencies $\alpha(T)$ [Eq. (15)] or $C_P(T)$ [Eq. (16)], where, for each pair of two neighboring experimental points, the changes in volume expansion, $\Delta\alpha(T)$, or heat capacity, $\Delta C_P(T)$, are strongly related to changes in compressibility, $\Delta\kappa(T)$.

In fact, to obtain $\Delta\kappa(T)$ by using $\Delta C_P(T)$, we should know the magnetic contribution to the total heat capacity. The temperature dependence of specific heat of $LaFe_{11.4}Si_{1.6}$ is shown in the inset of Fig. 7. It is well

known that the heat capacity of metals can be considered as the sum of independent electronic, lattice (phonon), and magnetic contributions:

$$C_P(H,T) = C_{\rm el}(T) + C_{\rm ph}(T) + C_{\rm mag}(H,T) \qquad (17)$$

The electron and phonon contributions to the specific heat can be calculated as [44]:

$$C_{\rm el+ph} = \gamma T + 9NR\left(\frac{T}{\Theta_D}\right)^3 \int_0^{\Theta_D/T} \frac{x^4 e^x}{(e^x-1)^2} dx, \qquad (18)$$

where the first term represents the electronic heat capacity and the second term corresponds to the phonon Debye contribution; γ is the Sommerfeld coefficient; Θ_D is the Debye temperature; N is the number of atoms per formula unit; R is the universal gas constant; and $x \equiv h\nu \big/ k_B T$, where ν is phonon frequency. In Fig. 7 (inset), both lattice and electronic contributions obtained with $\gamma = 150\,\mathrm{mJ\,mol^{-1}\,K^{-2}}$ and $\Theta_D = 360\ K$ as a fitting parameters and $N = 14$ are shown as a blue line. The separated temperature dependence of magnetic specific heat $C_{\rm mag}$ obtained by subtraction of the lattice and electronic contributions from the experimental data is presented in the inset in Fig. 7(b) as the red shaded area.

The value of dT_C/dP can be estimated by using Eq. (7) with $\beta = 15$, $T_0 = 196$ K, and $\kappa_0 = 8.6 \times 10^{-3}$ GPa^{-1}, and it is found to be $dT_C/dP = 25.3 \times 10^{-9}$ K/Pa. Figure 7(b) shows the temperature dependences of $\kappa_0 + \kappa(T)$ calculated from Eqs. (15) (red circles) and (16) (blue circles). Both dependences have a clearly pronounced maximum in the region of the phase transition. The compressibility varies from 10×10^{-12} to 8.6×10^{-12} Pa^{-1} for ferromagnetic and paramagnetic states correspondingly through the peak value of 35×10^{-12} Pa^{-1} at T_C in zero magnetic field. These values and temperature behavior are in a good agreement with data reported in the literature [45–47]. Data obtained using x-ray analysis at temperatures of 160 and 260 K are also presented in Fig. 7(b) as stars. It can be seen that the obtained compressibility values using the Bean–Rodbell model agree with the x-ray diffraction data.

In principle, Eqs. (15) and (16) are obtained by using a so-called continuous approach. At the same time, for the first-order transition, the Clausius-Clapeyron equation can also be used. If the paramagnetic and ferromagnetic phases coexist during the first-order transition, one can write

$$G_{\rm FM}(H,T,P) = G_{\rm PM}(H,T,P). \qquad (19)$$

Since the transition occurs in a zero magnetic field, the total differential can be derived as follows:

$$V_{\rm FM}dP - S_{\rm FM}dT = V_{\rm PM}dP - S_{\rm PM}dT. \qquad (20)$$

From Eq. (19), it follows

$$\Delta V dP = \Delta S dT \qquad (21)$$

Multiplying both sides of Eq. (21) by $1/VdP^2$ and using Eqs. (12b) and (12c), one can obtain

$$\kappa = \alpha \frac{dT_C}{dP}, \qquad (22)$$

and

$$\Delta\kappa = \kappa_{\rm FM} - \kappa_{\rm PM} = \Delta\alpha \frac{dT_C}{dP}. \qquad (23)$$

In a similar way, multiplying both sides of Eq. (21) by $1/dT$ and using Eqs. (12b) and (12c):

$$\Delta\kappa = \left(\frac{dT_C}{dP}\right)^2 \left(\frac{C_{P_{\rm FM}}}{T_C V_{\rm FM}} - \frac{C_{P_{\rm PM}}}{T_C V_{\rm PM}}\right) \qquad (24)$$

It must be noted that, using the Clausius-Clapeyron Eq. (21), we can calculate only the difference between thermodynamic parameters before and after transitions. Using Eqs. (23) and (24), and assuming that $\kappa_0 = 8.6 \times 10^{-12}$ Pa^{-1}, $\Delta\kappa_{\rm FM} = 0.93 \times 10^{-12}$ Pa^{-1} and $\Delta\kappa_{\rm PM} = 0.27 \times 10^{-12}$ Pa^{-1}, respectively [Fig. 7(b), orange and green triangles].

E. Magnetovolume coupling constant

For further calculation of $M(T)_P$ dependencies, one more quantity, characterizing the magnetoelastic interaction, should be estimated: the magnetovolume coupling constant, $C_{\rm MV}$. To describe the magnetovolume effect in La(Fe, Si)13 with a first-order phase transition, local-moment volume magnetostriction theory, developed by Callen and Callen [48], and that specified using the Stoner band model [49,50], can be applied. According to this theory, the spontaneous volume magnetostriction, $\omega(T)_H$, can be described as

$$\omega(T)_H = \kappa C_{\rm MV} M^2(T), \qquad (25)$$

where κ is the compressibility, $C_{\rm MV}$ is a magnetovolume coupling constant, and $M(T)$ is bulk magnetization.

The magnetovolume coupling coefficient, $\kappa C_{\rm MV}$, is equal to the slope of ω versus M^2 dependence [see Fig. 8(a)]. The volume magnetostriction in both paramagnetic and ferromagnetic states shows a linear dependence on the square of the magnetization, although the magnetovolume coupling coefficient in the ferromagnetic state ($\kappa C_{\rm MV} = 0.24\%/\mu_B{}^2$) is smaller than that in the paramagnetic state ($\kappa C_{\rm MV} = 0.53\%/\mu_B{}^2$). The temperature dependencies of the magnetovolume coupling coefficient $\kappa C_{\rm MV}$ (T) are shown in Fig. 8(b).

The fact that $\kappa C_{\rm MV}$ can be significantly different in ferromagnetic and paramagnetic states is known in the literature. A similar difference in $\kappa C_{\rm MV}$ between LuCo2 paramagnetic compound and Lu(CoxGa1$_x$)2 ($x = 0.09$

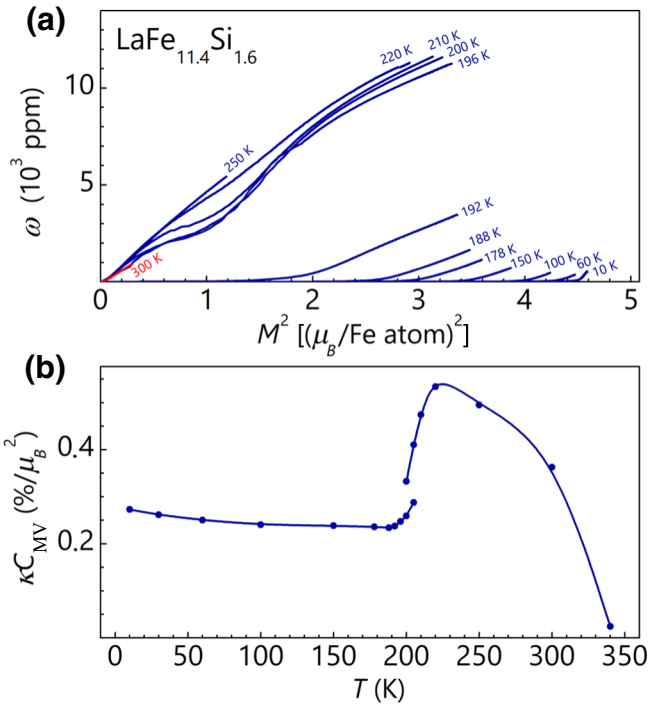

FIG. 8. (a) ω versus M^2 plots at different temperatures and (b) temperature dependence of magnetovolume coupling coefficient of $LaFe_{11.4}Si_{1.6}$ sample.

and 0.12) ferromagnetic compounds was obtained by Goto and Bartashevich from the volume magnetostriction measurements [51]: the value of κC_{MV} in the paramagnetic state is twice as large as that in the ferromagnetic state at 4.2 K for the sample with $x = 0.09$. According to Takahashi theory [52], they discussed the origin for the difference in κC_{MV} in terms of "zero-point fluctuation" of the magnetic moment, which associates the variation of κC_{MV} with changes in the spin-fluctuation spectrum. In Ref. [53], Fujita *et al.* explained that there was an increase in the magnetovolume coupling coefficient induced by the magnetic moment in the ferromagnetic state; hence, spin fluctuations are suppressed in the ferromagnetic state after the IEM transition. Thus, the influence of higher order terms on the magnetoelastic energy can qualitatively explain the change in the value of κC_{MV}.

F. Pressure dependence of β parameter

In the framework of the Bean-Rodbell model, we can successfully predict the experimental behavior of magnetization and volume changes taking place at the first-order phase transitions. However, this approach can be used only at ambient pressure. Indeed, the linear dependence of T_C on the volume [Eq. (1)] presumes that, with increasing pressure, the transition temperature should decrease linearly. In reality, the reduction of T_C under pressure demonstrates more complicated character and does not follow the linear law [38–40].

To adopt the Bean-Rodbell model for simulation of temperature dependencies of magnetization under pressure, we can use a pressure-dependent $\beta(P)$ parameter instead of β obtained in Sec. III B. For this purpose, we combine the Bean–Rodbell model with the spin fluctuation theory of the IEM transition based on the Landau expansion, according to which the pressure dependence of T_C over a wide pressure range obeys the following relation [54–56]:

$$T_C = \beta^* \sqrt{P_C - P}, \tag{26}$$

where P_C is the critical pressure at which $T_C = 0$ K. Such a defined parameter, β^*, is different from the corresponding β of the Bean-Rodbell model and, by analogy with Eq. (1), describes how T_C decreases with pressure.

Taking the pressure derivative of Eq. (26) and substituting the obtained result into Eq. (7), we can obtain the following formula for the determination of the pressure dependence of parameter $\beta(P)$:

$$\beta = \frac{1}{2\kappa T_0} \frac{\beta^*}{\sqrt{P_C - P}}. \tag{27}$$

In turn, in Ref. [54], parameter β^* was derived as

$$\beta^* \cong \sqrt{\frac{\kappa C_{MV}}{|b|\delta}}. \tag{28}$$

The coefficient b is determined from $M(H)_T$ dependencies using the following magnetic equation of state: $B = a(T)M + b(T)M^3 + c(T)M^5$. The parameter δ is the proportional coefficient of the relation $\xi(T)^2 = \Delta T^2$ [57], where $\xi(T)$ describes the intensity of thermal fluctuations. Thus, the value of Δ is related to the energy distribution of the spin-fluctuation spectrum. Direct observation of the thermal variation of $\xi(T)^2$ is difficult; however, the following relation between the temperature dependence of the critical field, $\mu_0 H_C$, of the itinerant electron magnetic transition and the thermal variation of $\xi(T)^2$ [39] can be used:

$$\mu_0 H_C = \Delta M_{ind}(b\delta) T^2, \tag{29}$$

where ΔM_{ind} is the difference in magnetic moments of paramagnetic and ferromagnetic phases observed at the IEM transition. Combining Eqs. (28) and (29), one can get the expression for β^* in the following form:

$$\beta^* \cong \sqrt{\frac{\kappa C_{MV} \Delta M_{ind} T^2}{\mu_0 H_C} \times 10^{-9}}. \tag{30}$$

Using the value of $\kappa C_{MV} = 0.34\%/\mu_B{}^2$, which is found in Sec. III E, together with the change in magnetic moment,

$\Delta M_{\rm ind} = 0.52\ \mu_B$, at critical field $\mu_0 H_C = 0.5$ T obtained at $T = 202$ K [see Figs. 8(b) and 4(a)], the parameter $\beta^* = 0.0038$ K/Pa$^{1/2}$ is calculated by using Eq. (30). This value is close to that of experimental data reported in the literature for La(Fe, Si)13 compounds (see, e.g., [39]).

Now, we have almost the whole set of quantities, except the critical pressure, P_C, to determinate the pressure dependence of parameter β within the Bean–Rodbell model by using Eq. (27). P_C can be calculated as follows [54]:

$$P_C = \frac{b^2(0)}{2\kappa C_{\rm MV} c(0)} \left| \frac{3}{16} - \frac{a(0)c(0)}{b^2(0)} \right| \times 10^9, \qquad (31)$$

where $a(0)$, $b(0)$, and $c(0)$ are the Landau coefficients derived from approximation of the $M(H)_T$ curve by the equation of state $B = a(T)M + b(T)M^3 + c(T)M^5$ at low temperature T.

Using Eq. (31), the value of critical pressure for $LaFe_{11.4}Si_{1.6}$ is calculated to be $P_C = 1.3 \pm 0.05$ GPa (the coefficients $a(0) = 4.81T/(\mu_B/\text{Fe})$, $b(0) = -4.53T/(\mu_B/\text{Fe})^3$, and $c(0) = 0.94T/(\mu_B/\text{Fe})^5$ are found at $T = 10$ K, $\kappa C_{\rm MV} = 0.28\%/\mu_B{}^2$), which agrees with previous data reported in the literature [54].

The calculated pressure dependence $\beta(P)$ obtained from Eq. (26) is presented in Fig. 9(a) (solid blue circles). As shown on the plot, with increasing applied pressure, the values of the β parameter are rising due to enhancing the first-order character of the phase transition. The obtained $\beta(P)$ allows us to calculate the pressure behavior of the Curie point, $T_C(P)$, according to Eq. (4) [see Fig. 9(b), orange symbols].

G. Verification of the model

For verification of the developed model, direct measurements of magnetization under external pressure (up to $P = 1$ GPa) are carried out on the same sample as that used for the simultaneous measurement of magnetization and the magnetovolume effect (Figs. 4 and 5). The experimental temperature dependencies of $M(T)_{P,H}$ detected for five selected pressures are shown in Fig. 10(a) (solid lines). Using Eq. (5), the temperature dependences of reduced spontaneous magnetization are found. The simulated $\sigma(T)_{P,H}$ dependencies for different pressures are presented in Fig. 10(a) (dashed red lines).

The small misfit in the Curie point in the low-pressure region is caused by a discrepancy in the β parameter estimation. The comparative analysis of the latter is exposed in Fig. 9(a). The corresponding experimental values (open symbols) are calculated according to Eq. (7) for five selected pressures using $M(H)_{P,T}$. The error in the β parameter evaluation is mainly caused by variation of the β^* parameter with temperature. As shown in Fig. 10(b),

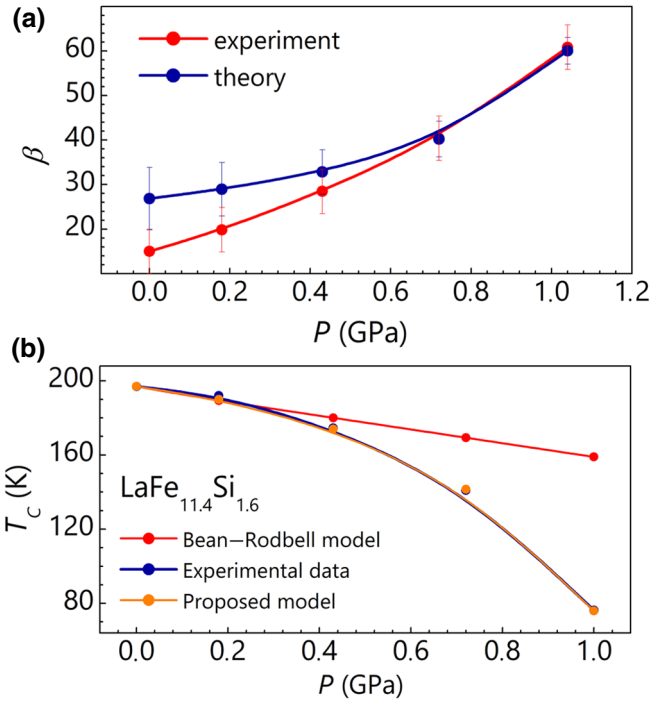

FIG. 9. (a) Pressure dependences of β parameter from experimental data for $LaFe_{11.4}Si_{1.6}$ sample (open red circles) and calculated values (filled blue circles). (b) Curie temperature of $LaFe_{11.4}Si_{1.6}$ under different pressures: experimental data (blue circles) and those calculated with conventional (red circles) and modified Bean and Rodbell models (orange circles).

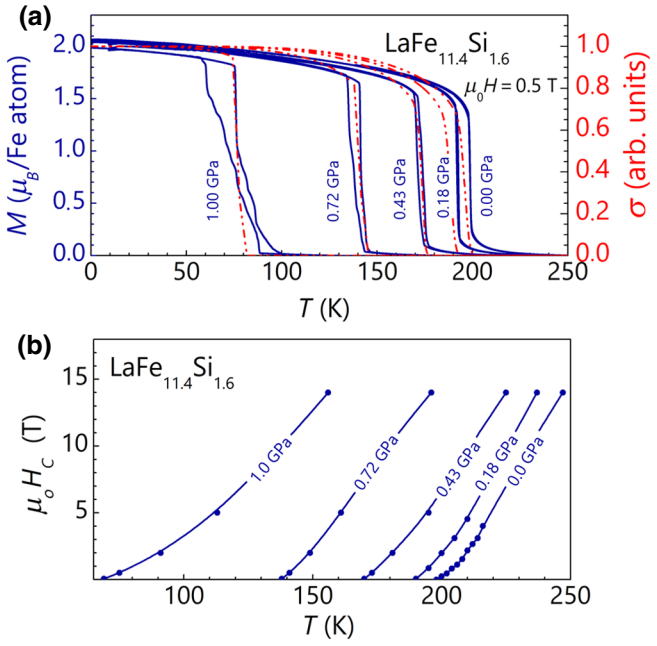

FIG. 10. (a) Temperature dependence of magnetization (solid lines) and calculated temperature dependence of reduced magnetization (dash lines) for $LaFe_{11.6}Si_{1.4}$ samples under different pressures. (b) Temperature dependence of critical field of phase transition for $LaFe_{11.4}Si_{1.6}$ under different pressures.

due to relatively inalterable nature of $d(\mu_0 H_C)/dT$ over the wide range of applied pressure, $P < 1$ GPa [58], the deviation in β^* values obtained with Eq. (30) is less than 15% for $T > T_C$ and $P < 1$ GPa.

The experimental pressure dependence of the Curie temperature, $T_C(P)$, is depicted in Fig. 9(b) as solid blue circles. In the framework of the developed model, we succeed in reproducing the real square-root character of $T_C(P)$. At the same time, our data are significantly different from that of $T_C(P)$ obtained by using the conventional Bean-Rodbell model (red symbols). Obviously, our proposed approach provides a more realistic $T_C(P)$, which is much closer to the experimental data (dark blue symbols) than the values predicted by the Bean-Rodbell model.

IV. CONCLUSION

Here, we develop a comprehensive experimental-theoretical approach for the understanding of multistimuli-responsive caloric materials with first-order transitions and for the optimization of their functional properties. First, we design and build the MaRS that can provide a self-consistent set of parameters, such as simultaneously measured magnetization, M; volume magnetostriction, $\omega(H)_T$; and temperature of the sample, T. Second, using as an example the magnetocaloric $LaFe_{11.4}Si_{1.6}$ compound with a first-order field-induced transition, and based on the Bean-Rodbell model, we develop a model that allows us to describe analytically the behavior of magnetization under different pressures using our $M(T)$ and $\omega(T)$ dependencies measured simultaneously at ambient pressure.

Our model also enables estimation of the temperature dependence of compressibility, $\kappa(T)$, without carrying out complex and time-consuming XRD measurements of lattice parameters under pressure. Additional parameters, such as the thermal expansion coefficient, $\alpha(T)$, and magnetoelastic interaction or effective magnetovolume coupling constant, C_{MV}, can also be determined within the framework of our approach.

For verification of the model, direct measurements of magnetization under external pressure (up to $P = 1$ GPa) are carried out on the same sample as that used for the simultaneous measurement of magnetization and the magnetovolume effect. A comparison of simulated $M(T)_P$ dependencies with experimental $M(T)_P$ confirms that our approach provides a more realistic behavior of the transition temperature under pressure, $T_C(P)$, than that of $T_C(P)$ predicted by the original Bean–Rodbell model. Thus, our approach is more suitable for predicting the behavior of multistimuli-responsive caloric materials with first-order transitions under changes of both magnetic field and pressure.

Finally, our model can be easily extended to a large class of advanced magnetic materials that exhibit a magnetostructural first-order transition (Fe-Rh, Gd5Si2 Ge2, Mn-Fe-P-Si, Heusler alloys, etc.) to reveal the driving forces and mechanisms governing the field-induced transformations in these material systems. Moreover, the comprehensive experimental-theoretical technique evolved here can provide a basic starting point for creating realistic models predicting the magnetocaloric effect under additional stimuli, such as stress and electric field.

ACKNOWLEDGMENTS

This work is supported by the European Research Council (ERC) under the European Union's Horizon 2020 research and innovation program (Grant No. 743116 project Cool Innov), by the Deutsche Forschungsgemeinschaft (DFG, German Research Foundation) – Grant No. 405553726 – TRR 270. D. K. gratefully acknowledges the financial support of the Ministry of Education and Science of the Russian Federation in the framework of Increase Competitiveness Program of NUST "MISiS" (No K3-2017-069), implemented by a governmental decree dated March 16, 2013 N 211 and the Russian Science Foundation (Grant No. 18-42-06201).

[1] T. Gottschall, K. P. Skokov, M. Fries, A. Taubel, I. Radulov, F. Scheibel, D. Benke, S. Riegg, and O. Gutfleisch, Making a cool choice: The materials library of magnetic refrigeration, Adv. Energy Mater. **9**, 1901322 (2019).

[2] O. Gutfleisch, T. Gottschall, M. Fries, D. Benke, I. Radulov, K. P. Skokov, H. Wende, M. Gruner, M. Acet, P. Entel, and M. Farle, Mastering hysteresis in magnetocaloric materials, Philos. Trans. R. Soc. A Math. Phys. Eng. Sci. **374**, 20150308 (2016).

[3] F. Scheibel, T. Gottschall, A. Taubel, M. Fries, K. P. Skokov, A. Terwey, W. Keune, K. Ollefs, H. Wende, M. Farle, M. Acet, O. Gutfleisch, and M. E. Gruner, Hysteresis design of novel magnetocaloric materials - from basic mechanisms to applications, Energy Technol **6**, 1397 (2018).

[4] A. Smith, C. R. H. Bahl, R. Bjørk, K. Engelbrecht, K. K. Nielsen, and N. Pryds, Materials challenges for high performance magnetocaloric refrigeration devices, Adv. Energy Mater. **2**, 1288 (2012).

[5] V. Franco, J. S. Blázquez, J. J. Ipus, J. Y. Law, L. M. Moreno-Ramírez, and A. Conde, Magnetocaloric effect: From materials research to refrigeration devices, Prog. Mater. Sci. **93**, 112 (2018).

[6] J. Steven Brown and P. A. Domanski, Review of alternative cooling technologies, Appl. Therm. Eng. **64**, 252 (2014).

[7] K. Klinar, U. Tomc, B. Jelenc, S. Nosan, and A. Kitanovski, New frontiers in magnetic refrigeration with high oscillation energy-efficient electromagnets, Appl. Energy **236**, 1062 (2019).

[8] A. Kitanovski, J. Tušek, U. Tomc, U. Plaznik, M. Ožbolt, and A. Poredoš, *Magnetocaloric Energy Conversion* (Springer International Publishing, Switzerland, 2015).

[9] A. Kitanovski, P. W. Egolf, and A. Poredos, Rotary magnetic chillers with permanent magnets, Int. J. Refrig. **35**, 1055 (2012).

[10] T. Gottschall, M. D. Kuz'min, K. P. Skokov, Y. Skourski, M. Fries, O. Gutfleisch, M. G. Zavareh, D. L. Schlagel, Y. Mudryk, V. Pecharsky, and J. Wosnitza, Magnetocaloric effect of gadolinium in high magnetic fields, Phys. Rev. B **99**, 134429 (2019).

[11] S. Taskaev, V. Khovaylo, D. Karpenkov, I. Radulov, M. Ulyanov, D. Bataev, A. Dyakonov, D. Gunderov, K. Skokov, and O. Gutfleisch, Plastically deformed Gd-X (X=Y, In, Zr, Ga, B) solid solutions for magnetocaloric regenerator of parallel plate geometry, J. Alloys Compd. **754**, 207 (2018).

[12] O. Gutfleisch, M. A. Willard, E. Bruck, C. H. Chen, S. G. Sankar, and J. P. Liu, Magnetic materials and devices for the 21st century: Stronger, lighter, and more energy efficient, Adv. Mater. **23**, 821 (2011).

[13] V. Basso, M. Piazzi, C. Bennati, and C. Curcio, Hysteresis and phase transition kinetics in magnetocaloric materials, Phys. Status Solidi **255**, 1700278 (2018).

[14] Ö Çakır and M. Acet, Reversibility in the inverse magnetocaloric effect in Mn 3 GaC studied by direct adiabatic temperature-change measurements, Appl. Phys. Lett. **100**, 202404 (2012).

[15] F. Guillou and E. Brück, Tuning the metamagnetic transition in the (Co, Fe)MnP system for magnetocaloric purposes, J. Appl. Phys. **114**, 143903 (2013).

[16] K. P. Skokov, K. H. Müller, J. D. Moore, J. Liu, A. Y. Karpenkov, M. Krautz, and O. Gutfleisch, Influence of thermal hysteresis and field cycling on the magnetocaloric effect in $LaFe_{11.6}Si_{1.4}$, J. Alloys Compd. **552**, 310 (2013).

[17] A. Chirkova, K. P. Skokov, L. Schultz, N. V. Baranov, O. Gutfleisch, and T. G. Woodcock, Giant adiabatic temperature change in FeRh alloys evidenced by direct measurements under cyclic conditions, Acta Mater. **106**, 15 (2016).

[18] T. Gottschall, A. Gràcia-Condal, M. Fries, A. Taubel, L. Pfeuffer, L. Mañosa, A. Planes, K. P. Skokov, and O. Gutfleisch, A multicaloric cooling cycle that exploits thermal hysteresis, Nat. Mater. **17**, 929 (2018).

[19] J. Liu, T. Gottschall, K. P. Skokov, J. D. Moore, and O. Gutfleisch, Giant magnetocaloric effect driven by structural transitions, Nat. Mater. **11**, 620 (2012).

[20] A. Gràcia-Condal, E. Stern-Taulats, A. Planes, and L. Mañosa, Caloric response of Fe49Rh51 subjected to uniaxial load and magnetic field, Phys. Rev. Mater. **2**, 084413 (2018).

[21] X. Moya, S. Kar-Narayan, and N. D. Mathur, Caloric materials near ferroic phase transitions, Nat. Mater. **13**, 439 (2014).

[22] E. Stern-Taulats, T. Castán, L. Mañosa, A. Planes, N. D. Mathur, and X. Moya, Multicaloric materials and effects, MRS Bull. **43**, 295 (2018).

[23] L. Mañosa and A. Planes, Materials with giant mechanocaloric effects: Cooling by strength, Adv. Mater. **29**, 1603607 (2017).

[24] E. Z. Valiev, I. F. Berger, V. I. Voronin, V. A. Glazkov, A. A. Kaloyan, and K. M. Podurets, Effect of hydrostatic pressure on the magnetic and lattice properties of the ferromagnet La(Fe0.86Si0.14)13, Phys. Solid State **56**, 14 (2014).

[25] M. G. Zavareh, Y. Skourski, K. P. Skokov, D. Y. Karpenkov, L. Zvyagina, A. Waske, D. Haskel, M. Zhernenkov, J. Wosnitza, and O. Gutfleisch, Direct Measurement of the Magnetocaloric Effect in la (Fe, Si, Co)13 Compounds in Pulsed Magnetic Fields, Phys. Rev. Appl. **8**, 14037 (2017).

[26] A. Fujita, K. Fukamichi, K. Koyama, and K. Watanabe, X-ray diffraction study in high magnetic fields of magnetovolume effect in itinerant-electron metamagnetic La(Fe0.88Si0.12)13 compound, J. Appl. Phys. **95**, 6687 (2004).

[27] A. K. Pathak, P. Basnyat, I. Dubenko, S. Stadler, and N. Ali, Influence of the small substitution of Z=Ni, Cu, Cr, V for Fe on the magnetic, magnetocaloric, and magnetoelastic properties of $LaFe_{11.4}Si_{1.6}$, J. Magn. Magn. Mater. **322**, 692 (2010).

[28] E. Callen and H. B. Callen, Magnetostriction, forced magnetostriction, and anomalous thermal expansion in ferromagnets, Phys. Rev. **139**, A455 (1965).

[29] A. Fujita, S. Fujieda, Y. Hasegawa, and K. Fukamichi, Itinerant-electron metamagnetic transition and large magnetocaloric effects in La(FexSi1-x)13 compounds and their hydrides, Phys. Rev. B **67**, 104416 (2003).

[30] J. Liu, J. D. Moore, K. P. Skokov, M. Krautz, K. Löwe, A. Barcza, M. Katter, and O. Gutfleisch, Exploring La(Fe, Si)13 -based magnetic refrigerants towards application, Scr. Mater. **67**, 584 (2012).

[31] J. Y. Law, V. Franco, L. M. Moreno-Ramírez, A. Conde, D. Y. Karpenkov, I. Radulov, K. P. Skokov, and O. Gutfleisch, A quantitative criterion for determining the order of magnetic phase transitions using the magnetocaloric effect, Nat. Commun. **9**, 2680 (2018).

[32] K. G. Sandeman, Magnetocaloric materials: The search for new systems, Scr. Mater. **67**, 566 (2012).

[33] S. K. Banerjee, On a generalized approach to first and second order magnetic transitions, Phys. Lett. **12**, 16 (1964).

[34] R. W. De Blois and D. S. Rodbell, Magnetic first-order phase transition in single-crystal MnAs, Phys. Rev. **130**, 1347 (1963).

[35] C. P. Bean and D. S. Rodbell, Magnetic disorder as a first-order phase transformation, Phys. Rev. **126**, 104 (1962).

[36] D. S. Rodbell and C. P. Bean, Some magnetic first-order transitions, J. Appl. Phys. **33**, 1037 (1962).

[37] H. Klimker and M. Rosen, Elastic properties of polycrystalline rare earth-cobalt laves compounds, J. Magn. Magn. Mater. **7**, 361 (1978).

[38] Y. Sun, Z. Arnold, J. Kamarad, G. J. Wang, B. G. Shen, and Z. H. Cheng, Pressure enhancement of the giant magnetocaloric effect in $LaFe_{11.6}Si_{1.4}$, Appl. Phys. Let. **89**, 172513 (2006).

[39] H. Yako, S. Fujieda, A. Fujita, and K. Fukamichi, Pressure effect on the curie temperature of (La(Fe0.88Si0.12 − yAly)13, J. of Phys. Conf. Ser **266**, 012023 (2011).

[40] A. Fujita, S. Fujieda, K. Fukamichi, H. Mitamura, and T. Goto, Itinerant-electron metamagnetic transition and large magnetovolume effects in(La(FexSi1 − x)13 compounds, Phys. Rev. B **65**, 014410 (2001).

[41] L. Caron, Z. Q. Ou, T. T. Nguyen, D. T. Cam Thanh, O. Tegus, and E. Brück, On the determination of the magnetic entropy change in materials with first-order transitions, J. Magn. Magn. Mater. **321**, 3559 (2009).

[42] A. Chirkova, K. P. Skokov, L. Schultz, N. V. Baranov, O. Gutfleisch, and T. G. Woodcock, Giant adiabatic temperature change in FeRh alloys evidenced by direct measurements under cyclic conditions, Acta Mater. **106**, 15e21 (2016).

[43] H. Neves Bez, H. Yibole, A. Pathak, Y. Mudryk, and V. K. Pecharsky, Best practices in evaluation of the magnetocaloric effect from bulk magnetization measurements, J. Magn. Magn. Mater. **458**, 301 (2018).

[44] E. Gopal, *The International Cryogenics Monograph Series*, edited by Mendelssohn K., Timmerhaus K. D. (Heywood, London, 1966).

[45] M. P. Grazhdankina, First-Order magnetic phase transitions, Usp. Fiz. Nauk **96**, 291 (1968).

[46] H. Klimker, M. P. Dariel, and M. Rosen, Temperature and magnetic field dependence of the elastic properties of rare earth-cobalt laves phase compounds, J. Phys. Chem. Solids **40**, 195 (1979).

[47] E. Z. Valiev and V. A. Kazantsev, Magnetocaloric effect in(La(FexSi1 − x)13, JETP **113**, 1000 (2011).

[48] E. Callen and H. B. Callen, Magnetostriction, forced magnetostriction, and anomalous thermal expansion in ferromagnets, Phys. Rev. **139**, A455 (1965).

[49] E. P. Wohlfarth, Forced magnetostriction in the band model of magnetism, J. Phys. C Solid State Phys. **2**, 68 (1969).

[50] E. P. Wohlfarth, Thermodynamic aspects of itinerant electron magnetism, Physica B+ C **91**, 305 (1977).

[51] T. Goto and M. I. Bartashevich, Magnetovolume effects in metamagnetic itinerant-electron systems, J. Phys. Condens. Matter **10**, 3625 (1998).

[52] Y. Takahashi, Magneto-volume effects in weakly ferromagnetic metals, J. Phys. Condens. Matter **2**, 8405 (1990).

[53] A. Fujita, K. Fukamichi, K. Koyama, and K. Watanabe, X-ray diffraction study in high magnetic fields of magnetovolume effect in itinerant-electron metamagnetic La(Fe0.88Si0.12)13 compound, J. Appl. Phys. **95**, 6687 (2004).

[54] A. Fujita, K. Fukamichi, M. Yamada, and T. Goto, Pressure-induced anomalies in itinerant-electron metamagnetic properties around the critical end point in La(Fe0.89Si0.11)13, Phys. Rev. B **73**, 104420 (2006).

[55] C. Pfleiderer, G. J. McMullan, S. R. Julian, and G. G. Lonzarich, Magnetic quantum phase transition in MnSi under hydrostatic pressure, Phys. Rev. B **55**, 8330 (1997).

[56] C. Pfleiderer, D. Reznik, L. Pintschovius, H. V. Löhneysen, M. Garst, and A. Rosch, Partial order in the non-Fermi-liquid phase of MnSi, Nature **427**, 227 (2004).

[57] H. Yamada, Metamagnetic transition and susceptibility maximum in an itinerant-electron system, Phys. Rev. B **47**, 11211 (1993).

[58] A. Fujita, K. Fukamichi, M. Yamada, and T. Goto, Influence of pressure on itinerant electron metamagnetic transition in compounds, J. Appl. Phys. **93**, 7263 (2003).